RSC Advances

This is an *Accepted Manuscript*, which has been through the Royal Society of Chemistry peer review process and has been accepted for publication.

Accepted Manuscripts are published online shortly after acceptance, before technical editing, formatting and proof reading. Using this free service, authors can make their results available to the community, in citable form, before we publish the edited article. This *Accepted Manuscript* will be replaced by the edited, formatted and paginated article as soon as this is available.

You can find more information about *Accepted Manuscripts* in the Information for Authors.

Please note that technical editing may introduce minor changes to the text and/or graphics, which may alter content. The journal's standard Terms & Conditions and the Ethical guidelines still apply. In no event shall the Royal Society of Chemistry be held responsible for any errors or omissions in this *Accepted Manuscript* or any consequences arising from the use of any information it contains.

ROYAL SOCIETY OF CHEMISTRY

www.rsc.org/advances

Please do not adjust margins

Journal Name

ARTICLE

Competing mechanisms for the reaction of dichloropropynylborane with 2-*tert*-butylbutadiene. Diels-Alder reaction *versus* alkynylboration

Received 00th January 20xx,
Accepted 00th January 20xx

DOI: 10.1039/x0xx00000x

www.rsc.org/

Margarita M. Vallejos,[*a] and Silvina C. Pellegrinet[*b]

Density functional theory and the quantum theory of atoms in molecules approach were used to study two competing process: the Diels-Alder reaction (DA) and the 1,4-alkynylboration (AB) between dichloropropynylborane (**1**) and 2-*tert*-butylbutadiene (**2**) in dichloromethane. We analyzed several reaction pathways related with such reactions for both orientations (*meta* and *para*). The stepwise mechanisms for the two competitive reactions share the first step that leads to an intermediate zwitterionic structure. The second step is more favorable for the reaction occurring via **TSC-m** that leads to the *meta* enyne product 5, which is the kinetic product. The formation of the *meta* DA product cannot be explained through a direct cycloaddition, due to the higher activation free energy of the associated transition structure (**TSB-m).** An alternative transition structure with [4 + 3] character (**TSD-m**) that connects the *meta* enyne **5** with the *meta* cycloadduct 3 was found. We propose that at longer reaction times, **5** rearranges to the thermodynamic product **3** *via* **TSD-m** passing by a six-membered ring structure and a seven-membered ring structure. The topological analysis of the charge density along the selected reaction coordinates provided some understanding on the intriguing competitive reactions.

Introduction

Alkynyl boron reagents have shown great versatility as building blocks in several cycloaddition reactions leading to a wide variety of compounds in a regioselective manner.[1-15] Moreover, the cycloaddition products can be used in subsequent reactions to obtain complex structures. Among these compounds, alkynylboranes have proved to be good dienophiles showing an unusual electronic preference for the *meta* products in Diels-Alder (DA) reactions. Singleton et al.[16] have reported that the DA reactions of (trimethylsilyl)ethynyl-9-BBN and acyclic dienes at 100 ºC lead to the corresponding 1,4-cyclohexadienes with predominance of the *meta* cycloadduct products consistent with the [4 atom + 3 atom] transition structure (TS). Other alkynyldialkylboranes were shown to be poor dienophiles due to their low reactivity while alkynyldihaloboranes were extremely reactive in cycloaddition reactions.[16] The DA reactions of alkynyldihaloboranes with isoprene as diene in hexanes at 25 ºC generated the cycloadducts in high yields and with complete *meta* regioselectivity. Interestingly, the reactions of alkynyldihaloboranes and 2-*tert*-butylbutadiene in dichloromethane afforded the *meta* DA cycloadduct, together with the product of 1,4-alkynylboration (AB) (Scheme 1).[17,18] The experimental outcome of these reactions indicated that the amount of alkynylboration product depends on the reaction time, the solvent and the structure of the reactants. On the basis of theoretical calculations, Singleton et al. proposed an unified mechanism for the DA reaction and the AB process through of a zwitterionic seven-membered ring species.[17]

[a.] *Área de Química Orgánica, Departamento de Química, Facultad de Ciencias Exactas y Naturales y Agrimensura, Universidad Nacional del Nordeste, Avda. Libertad 5460, (3400) Corrientes, Argentina. Phone/Fax: +54-379-4457996 int.104 E-mail: vallejos.marga@gmail.com*

[b.] *Instituto de Química Rosario (CONICET), Facultad de Ciencias Bioquímicas y Farmacéuticas, Universidad Nacional de Rosario, Suipacha 531, Rosario (2000), Argentina. Phone/Fax: +54-341-4370477 E-mail: pellegrinet@iquir-conicet.gov.ar*

Electronic Supplementary Information (ESI) available: MPWB1K/6-311++G(d,p) energies in DCM for reactants and products, QTAIM analysis along the selected reaction paths and B3LYP/6-311++G(d,p) computed total energies, unique frequency imaginary, and cartesian coordinates of the stationary points under study. See DOI: 10.1039/x0xx00000x

RSC Advances Accepted Manuscript

Please do not adjust margins

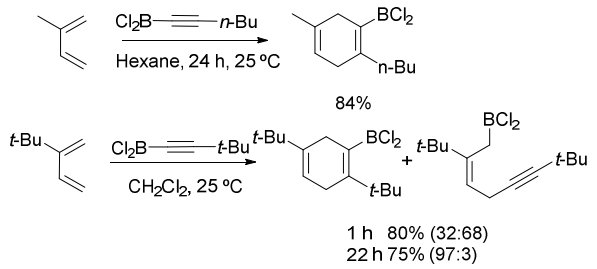

Scheme 1

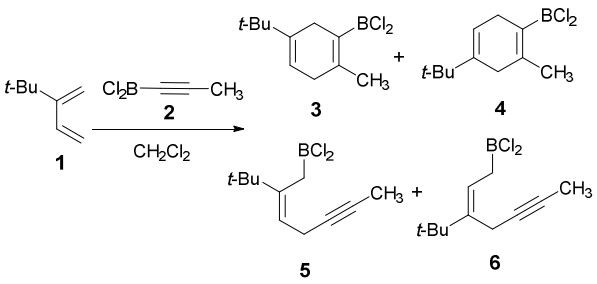

Scheme 2

Goodman et al. investigated the cycloaddition mechanism for a series of alkynyldihaloboranes and alkynyldialkylboranes with 1,3-butadiene using density functional theory (DFT) calculations.[19] Two different TSs connecting the reactants with the 1,4-cyclohexadienylborane products were found. The more energetically favored structure had classical [4 + 2] character with a C-B secondary orbital interaction while the other one showed strong [4 + 3] character. The TS corresponding to the concerted pathway for the direct AB was not found. Instead, a TS that connects the enyne product of the AB process with the DA product via a zwitterionic structure was located. These authors also studied the reaction of isoprene as a model of substituted systems, and dichloropropynylborane to provide further insight into the DA reaction and the AB pathways.[20] Again, two TSs were found for the cycloaddition, one of them showed a classical [4 + 2] structure with a significant C-B secondary orbital interaction, and the other TS had high [4 + 3] character and it was energetically favored for the *meta* mode of addition, which explained the experimental regioselectivity for similar systems. In addition, a direct AB pathway was found only for the *meta* orientation, predicting the formation only of the *meta* AB product whereas the *para* TS, when launched toward the reactants, lead to the cyclohexadienylborane product, as in the case of butadiene. These results provided more understanding into the origin of the AB process and explained the preferred formation of the DA cycloadduct. However, the formation of the *meta* enyne as the major product at short reaction times in dichlorometane observed with highly substituted systems and why the cycloadduct became the major product when the reaction was left for longer could not be completely rationalized.

Carreaux, Cossío and co-workers21 carried out an experimental and computational study on the mechanism of a related reaction, i.e., the thermal dimerization of 2-boryl-1,3-butadienes to provide insight into the evolution of the [4 + 3] TSs toward the [4 + 2] cycloadducts. This study indicated that in the initial stage of the reaction the σ-overlap between the 2p atomic orbitals is more stabilizing for the C–B secondary interaction than for the C–C counterpart, favoring the [4 + 3] pathway. However, beyond the TS, the C–C orbital interaction becomes more favorable and the [4+3] zwitterionic species easily falls to the [4 + 2] cycloadduct. In the same context, we carried out a detailed study in the framework of the quantum theory of ato in molecules (QTAIM)[22, 23] along the course of the DA reactions of isoprene with a set of vinylboranes, finding that the evolution of the [4 + 3] to the [4 + 2] structure observed in the *endo* pathway of the DA reaction with vinylborane occurs through of a conflict mechanism in which the C_1 and B atoms of the dienophile compete to become attached to the C_6 atom of the diene.[24]

In this work, we have studied the reaction of 2-*tert*-butylbutadiene (**1**) with dichloropropynylborane (**2**), in order to gain a better understanding on the competition between the DA cycloaddition and the AB process. Scheme 2 shows the structure of the four possible products: **3** and **4** correspond to the DA reaction, and **5** and **6** to the AB. As far as we know, in previous works dedicated to study on the regioselectivity of the DA reactions of alkynylboranes the solvent effect was not taken into account. In this study, the solvent effect was considered because this is one of the key factors in these processes.

The QTAIM,[22, 23] based on the topological analysis of the electron charge density allows one to understand the electronic structure of molecules and also the nature and properties of chemical bonds. The analysis based on QTAIM along the reaction paths connecting the stationary points has been successfully applied to rationalize the mechanism of chemical reactions, such as the DA reactions of unsaturated organoboron dienophiles,[25] the dimerization of cyclopentadiene,[26] the Cope rearrangement of 1,5-hexadiene,[27] pericyclic and pseudopericyclic reactions,[28-34] among others.[35] In the present study, we have performed a QTAIM analysis to gain a deeper insight into the charge distribution and the bonding changes associated with the competitive DA reaction and AB process.

Methodology

Density functional theory (DFT) calculations were carried out using the Becke3 Lee–Yang–Parr (B3LYP)[36, 37] functional with the 6-311++G(d,p) basis set. The B3LYP/6-311++G(d,p) level of theory is appropriate to obtain reliable geometries and energies for the study of cycloadditions.[38-42]

The geometries of the reactants, the intermediate structures, the TSs and the products were optimized without any constraints. Frequency calculations were performed to determine the nature of the stationary points: the TSs had one imaginary frequency and the reactants, the intermediate structures and the products had no imaginary frequencies. Solvent effects in dichloromethane (DCM) (ε_{DCM} = 8.93) were evaluated through full optimizations using the polarizable

RSC Advances Accepted Manuscript

This journal is © The Royal Society of Chemistry 20xx

continuum model (PCM)[43] as in the framework of self-consistent reaction field (SCRF).[44-46] Free energies were computed at 298.15 K and 1 atm in DCM.

Intrinsic reaction coordinate (IRC) paths were traced to verify the connectivity of the TSs with reactants or intermediate structures and products. Some structures on the reaction pathway were selected for electronic structure analyses. All computations were carried out with the Gaussian 09 suite of programs.[47]

For the QTAIM topological analysis, total electron densities of the selected structures on the IRC were calculated at the B3LYP/6-311++G(d,p) level of theory. The bond and atomic properties in the framework of the QTAIM theory were calculated using the AIMALL program.[48]

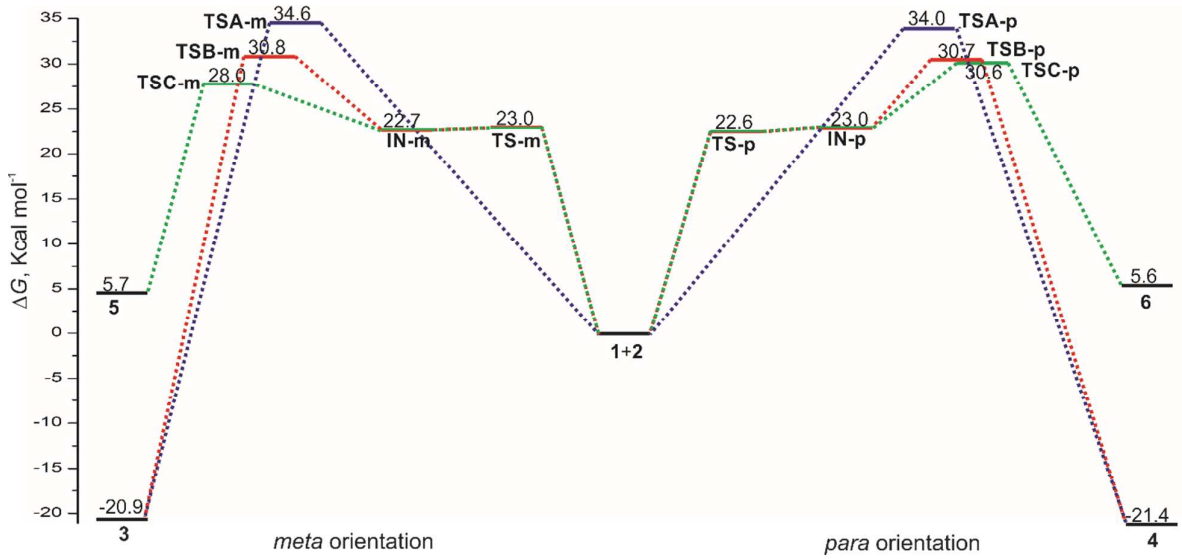

Fig. 1 Free energy profile for the reaction of **1** with **2** for the *meta* and *para* orientation modes. Paths **A** (blue) and **B** (red) correspond to the DA reaction and paths **C** (green) correspond to the AB process.

Results and discussion

Study of DA and AB pathways for the *meta* and *para* modes of addition between reactants 1 and 2

For each mode of addition of the reactants 1 and 2 (*meta* and *para*) three feasible pathways were found, two of them correspond to the DA reaction (paths **A** and **B**) and the other to the AB process (path **C**). The free energy profile for the reaction between **1** and **2** showing the located stationary points with their corresponding relative free energies in DCM is displayed in Fig. 1 (absolute energies in DCM are given in the ESI). The optimized geometries of the TSs and intermediate structures with selected bond distances are shown in Fig. 2.[49]

In path **A**, a TS for each orientation was found (**TSA-m** and **TSA-p**), which connects with the reactants and the corresponding DA product (**3** and **4**). Both paths correspond to a concerted DA mechanism. The length of the C_1-C_6 forming bond is larger than C_2-C_3 by 0.75 and 0.73 Å for **TSA-m** and **TSA-p**, respectively, indicating that these TSs are highly asynchronous and showing that the formation of the C_2-C_3 bond is more advanced than the C_1-C_6 bond. In both TSs the C_6-B distance is slightly shorter than C_1-C_6 forming bond reflecting the existence of notable C-B secondary orbital interactions. However, **TSA**s are classical [4 + 2] structures. In addition, **TSA**s have relatively high free energy barriers and **TSA-p** is lower in energy than **TSA-m** by 0.6 kcal mol^{-1} which does not explain the experimental regioselectivity and, in consequence, the reaction should follow another pathway towards the cycloadduct as it was previously proposed for the reaction of isoprene and dichlorovinylborane.[20]

The analysis of the stationary points of pathways **B** and **C**, associated with the DA reaction and the AB process, respectively indicates that these reactions take place through stepwise mechanisms. Both mechanisms share the first step of the reaction with a TS in which the boron atom of the dienophile portion approaches the C_6 atom of the diene (**TS-m** and **TS-p**) to yield the corresponding zwitterionic intermediate structures (**IN-m** and **IN-p**).

TS-m and **TS-p** show short C_6-B distances (2.11 and 2.02 Å, respectively) while the distances C_1-C_6, C_2-C_3 and C_1-C_3 are larger. **TS-p** has a lower free activation energy than **TS-m** (by 0.4 kcal mol^{-1}), however the formation of the [4 + 2] cycloadduct or AB product is determined by the second step of the reaction. In **IN-m** and **IN-p** the C_6-B distance becomes even shorter (1.78 and 1.86 Å, respectively). **IN-m** is slightly more stable than **IN-p** by 0.3 kcal mol^{-1} and in both cases the formation of these intermediates are endergonic (ΔG = 22.7

RSC Advances Accepted Manuscript

and 23.0 kcal mol^{-1} for **IN-m** and **IN-p**, respectively). **TSB**s, which lead to the [4 + 2] cycloadducts, have asynchronous structures being the C_1-C_6 distances 2.60 Å, and the C_2-C_3 distances 2.02 and 2.14 Å for **TSB-m** and **TSB-p**, respectively. Hence, **TSB-m** is slightly more asynchronous than **TSB-p**. In both TSs the C_6-B distance (~ 1.69 Å) is shorter than any of the forming bonds suggesting that **TSB**s have strong C-B secondary interactions, adopting [4 + 3] character.[24] As a consequence of the strong [4 + 3] C-B secondary interaction, **TSB**s are more stable than [4 + 2] **TSA**s.

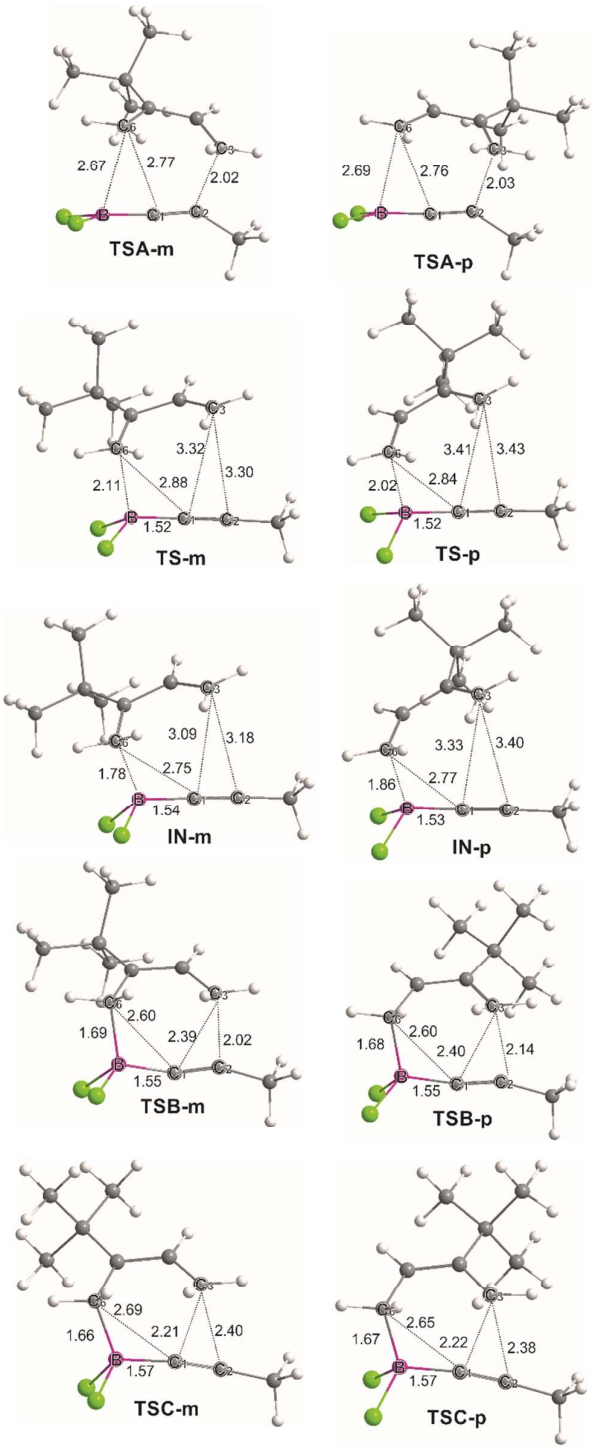

Fig. 2 Optimized geometries in DCM of the TSs and INs of the reaction of 2-*tert*-butylbutadiene (**1**) with dichloropropynylborane (**2**). Selected bond distances are given in Å.

In earlier studies on similar systems with butadiene as diene, no direct route from the reactants to the AB product was found, instead the TS connecting the cycloadduct and the AB product was located.[19] Also, with isoprene as diene a TS that leads to the AB product from the reactants was found only for the *meta* orientation while the *para* TS connected the AB and

RSC Advances Accepted Manuscript

This journal is © The Royal Society of Chemistry 20xx

Please do not adjust margins

DA products.[20] However, in our case IRC studies for **TSC-m** and **TSC-p** showed similar pathways, connecting the intermediates with the corresponding AB products **5** and **6**, respectively.

In **TSC**s the C_6-B bond distances are very short (~1.66 Å), with the B atom significantly pyramidalized, similar to **TSB**s, reflecting that the formation of the C_6-B bond is very advanced. In contrast with **TSB**s, the C_1-C_3 distances (2.21 and 2.22 Å for **TSC-m** and **TSC-p**, respectively) are shorter than the C_2-C_3 distances (2.40 Å for **TSC-m** and 2.38 Å for **TSC-p**) since the C_1-C_3 bonds are being formed. Also, the C_1-B distances in **TSC**s are slightly larger than in **TSB**s, which is consistent with the C_1-B bond breaking during the formation of the enyne products. In **TSB**s the dienophile portion is more bent (<BC_1C_2 ~166º and 169º) than in **TSC**s (<BC_1C_2 ~172º), and in the latter the dienophile portion is shifted with respect to the diene portion. In **TSB**s, a repulsive steric interaction between the methyl substituent on C_2 of the dienophile moiety and the atoms of the diene might operate and hence destabilize these structures, being the distance between the carbon of the methyl substituent and C_3 of 2.90 Å, while in **TSC**s these distances are larger (3.30 Å). Also, an attractive interaction between a chlorine atom attached to B of the dienophile and a hydrogen atom of the *t*-Bu substituent on C_5 of the diene might contribute to stabilize the *meta* TSs (**TSB-m** and **TSC-m**). In addition, the presence of a donating alkyl group on C_5 of the diene fragment stabilizes the incipient positive change developing after the boron attack, favoring the *meta* regioselectivity.[20]

TSC-m ($\Delta G^{\#}$ = 28.0 kcal mol^{-1}) is the most energetically favored structure among the TSs and determines the formation of the *meta* AB product under kinetic control. The free activation energy of **TSC-m** is lower than that of its *para* counterpart (**TSC-p**) by 2.6 kcal mol^{-1}, which predicts the almost exclusive formation of the *meta* enyne (99:1 mixture of the *meta*/*para* enyne products),[50] in agreement with the experimental regioselectivity of similar systems which showed that the *meta* enyne predominates at short reaction times while the *meta* cycloadduct becomes the major product when the reaction is left for longer (Scheme 1).[17] The free activation energies of **TSB-m** and **TSB-p** are very similar (30.8 and 30.7 kcal mol^{-1}, respectively) and these values are close to that of **TSC-p** thus, the formation of the *meta* cycloadduct could not take place through **TSB-m**, because if it happened a mixture of products would be obtained. These theoretical results do not explain the experimental outcome of the reaction.

Analysis of DA and AB reaction free energies

From Figure 1, the reaction free energies indicate that the *meta* and *para* DA products are more stable than the corresponding AB products by ~25 kcal mol^{-1}, and for both reactions regioisomeric products have similar free energies. These results support the fact that enyne **5** is the kinetic product of the reaction which predominates at short reaction times and also suggests that the formation of the [4 + 2] cycloadduct might take place under thermodynamic control. Note that the DA reaction is exergonic by ~ -21 kcal mol^{-1} while the AB process is endergonic by ~ 6 kcal mol^{-1}. Several groups have reported that the B3LYP functional is relatively accurate for kinetic data, but underestimates the exothermicity of the reaction.[51-53] The MPWB1K[54] functional proposed by the Truhlar group provides an improvement in the accuracy of the thermodynamic data. Therefore, in order to obtain reliable values of reaction energies we calculated the free energies of the reactants and the products in DCM using the proposed functional with the 6-311++G(d,p) basis set. Relative energies are displayed in Table 1 and the absolute energies are given in the ESI.

Table 1. MPWB1K/6-311++G(d,p) relative free energies (ΔG, in kcal mol^{-1}) computed at 298.15 K and 1 atm of the products of the reaction of **1** with **2**.

Product	ΔG (kcal mol^{-1})
3	-35.3
4	-35.4
5	-2.5
6	-1.7

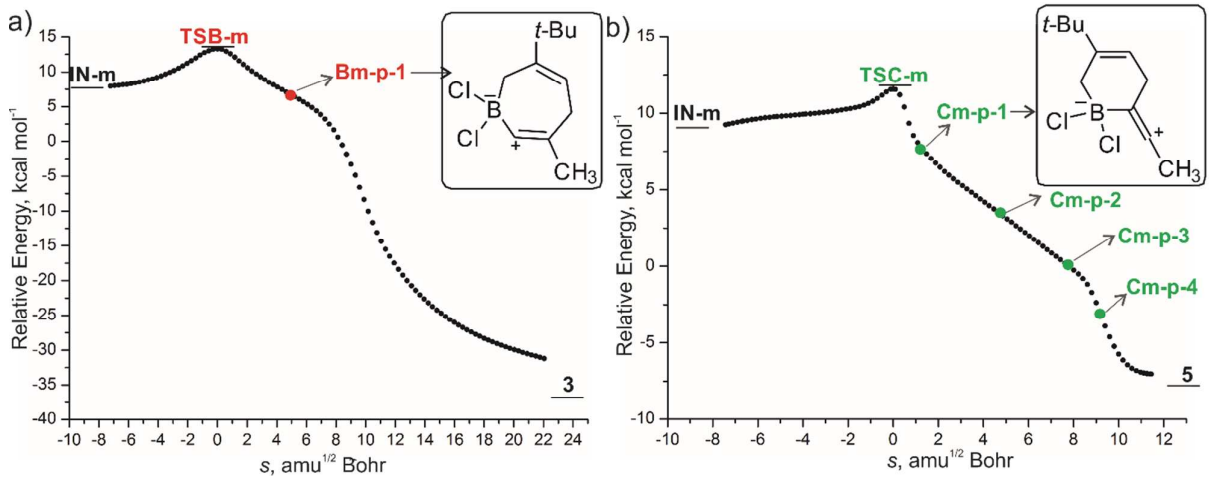

Please do not adjust margins

RSC Advances Accepted Manuscript

Fig. 3. Energy profiles along the intrinsic reaction coordinate for the *meta* channel of pathways a) **B** and b) **C** corresponding to the reaction between **1** and **2**. The zwitterionic structures are depicted and other selected points on the IRC are indicated.

The MPWB1K/6-311++G(d,p) free energies indicate that the AB processes are exergonic by -2.5 and -1.7 kcal mol^{-1}, and the formation of the *meta* and *para* cycloadducts is strongly exergonic by -35 kcal mol^{-1}. These results also predict that the cycloaddition reaction would be favored under thermodynamical control.

Analysis of the reaction coordinate associated with TSB-m and TSC-m. Conversion of the *meta* enyne to the *meta* DA cycloadduct

To explain the formation of cycloadduct **3** we figured that it could be formed from enyne **5**, as previously proposed.[17, 20] We analyzed the reaction coordinates associated with **TSB-m** and **TSC-m** which are depicted in Fig. 3. In the pathway that connects **TSB-m** with cycloadduct **3** there is a flat region in the reaction path corresponding with the seven-membered ring structure **Bm-p-1**. In early studies, a zwitterionic seven-membered ring which was associated with both the [4 + 3] cycloaddition and 1,4-alkynylboration pathways was also located and characterized.[19, 20]

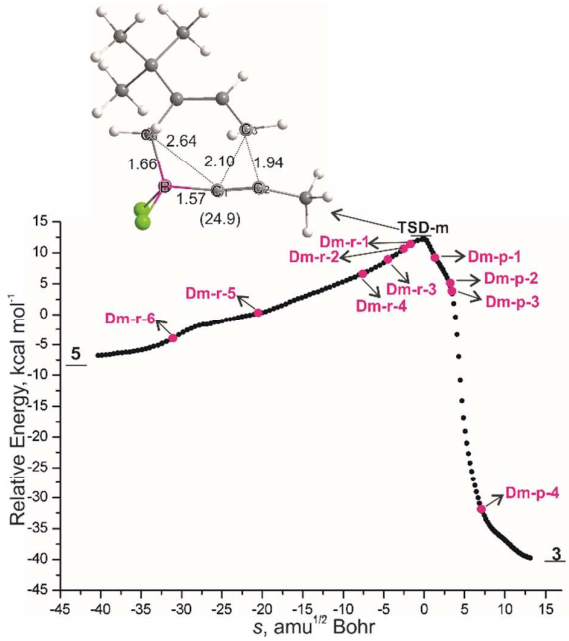

Fig.4 Energy profile along the intrinsic reaction coordinate associated with **TSD-m**. Optimized geometry in DCM of **TSD-m** together with some bond distances (in Å) and activation free energy (between parentheses, in kcal mol^{-1}) are included. Selected points on the IRC are indicated.

The IRC that connects **TSC-m** with enyne product **5** exhibits a rather flat area that corresponds to the six-membered ring structure **Cm-p-1**. It is worth noting that structures such as **Bm-p-1** and **Cm-p-1** are not stationary points. Because of this, we assumed that the zwitterionic six-membered ring **Cm-p-1**, which lays in a plateau region in the PES might rearrange to a seven-membered ring such as **Bm-p-1** and, then this species might lead to the *meta* DA cycloadduct which is more stable than the *meta* enyne product. Therefore, we propose that at longer reaction times the *meta* DA cycloadduct becomes the major product due to the rearrangement of the enyne *via* a zwitterionic six-membered ring and then a zwitterionic seven-membered ring. This proposal agrees with the early approach of an unified mechanism for the DA reaction and the AB through a zwitterionic seven-membered ring species though this intermediate has not been found.[17]

To prove this hypothesis, we performed a refined scan of the PES. Fortunately, we were able to locate a TS (**TSD-m**) that connects the enyne with the DA cycloadduct (Fig. 4).[55] Visualization of the vibration corresponding to the imaginary frequency clearly shows that C_3 shifts between C_1 and C_2. Interestingly, in the reaction coordinate from **TSD-m** to enyne **5** and to clycloadduct **3** flat areas were located corresponding to the six-membered ring structure (**Dm-r-4**) and seven-membered ring structure (**Dm-p-1**), respectively (see Fig. 4). In **TSD-m** the C_6-B, C_1-C_3 and C_2-C_3 bond distances (1.65, 2.10 and 1.94 Å, respectively) are shorter than those in **TSB-m** and **TSC-m**, indicating that the dienophile and diene portions are closer. **TSD-m** shows [4 + 3] character, as **TSB-m**, since the C_6-B distance is shorter than the C_1-C_6 distance (2.64 Å).[24] The free activation energy of **TSD-m** ($\Delta G^{\#}$ = 24.9 kcal mol^{-1}) is lower than that of **TSC-m**, therefore it supports our hypothesis that the formation of the DA cycloadduct from the enyne occurs under thermodinamic control. These results allowed us to explain the outcome of the reaction between **1** and **2** as displayed in the Scheme 3.

Topological QTAIM analysis

Several studies have shown that the topological QTAIM analysis along a reaction path is a powerful tool for characterizing reactions and understanding the nature of key interactions.[24, 25, 28-30] To further elucidate the electron density redistribution during the two competing processes and in an attempt to explain how the zwitterionic six-membered ring rearranges to the seven-membered ring structure leading to the DA cycloadduct from AB product, we carried out a topological analysis of charge density along the IRC coordinate associated with **TSC-m** and **TSD-m**. We analyzed the variations of several topological properties (the charge density ρ_b, its Laplacian $\nabla^2\rho_b$ and the ellypticity ε) at the bond critical point (bcp) in some bonds along the reaction path as well as the delocalization index (*DI*). Fig. 5 shows the contour plots of -$\nabla^2\rho_b$ superimposed on the molecular graphs of selected structures along the analyzed IRC including the topological properties for some bcps. The full QTAIM analysis is given in the ESI.

RSC Advances Accepted Manuscript

This journal is © The Royal Society of Chemistry 20xx

Please do not adjust margins

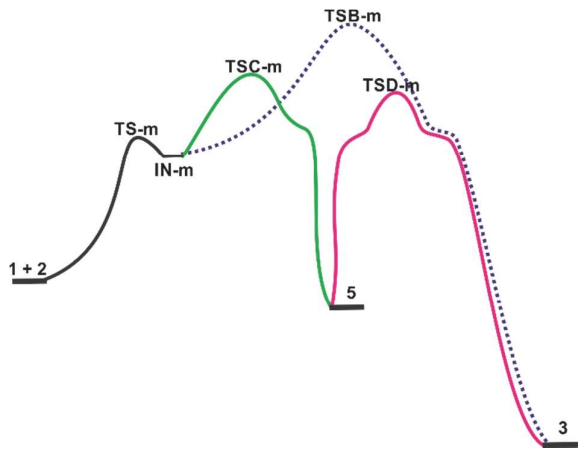

Scheme 3

Topological analysis of relevant points on the IRC of path C with *meta* orientation. Some significant information can be obtained from the QTAIM analysis along the two analyzed paths. In **TSC-m** the C_6-B bcp (ρ_b = 0.154 au., $\nabla^2\rho_b$ = -0.249 au.,ε = 0.04) and the C_1-B bcp (ρ_b = 0.159 au., $\nabla^2\rho_b$ = 0.057 au.,ε = 0.10) display the hallmarks of "shared-shell" or covalent interaction while the C_1-C_3 interaction is weaker and has "closed-shell" features (ρ_b = 0.053 au., $\nabla^2\rho_b$ = 0.068 au., ε = 0.41) (See Fig. 5). This can also be visualized in the contour plot -$\nabla^2\rho_b$ through the charge density distribution around the corresponding bcps. Hence, the C_6-B bond is practically formed at **TSC-m** and the breaking/formation of the C_1-B/C_1-C_3 bonds begins afterwards. C_1-C_3 σ-bond formation takes place just after **TSC-m**. In **Cm-p-1** the topological properties at C_1-C_3 bcp (ρ_b = 0.148 au., $\nabla^2\rho_b$ = -0.134 au., *DI* = 0.67 and ε = 0.09) are clearly indicative of a shared shell interaction, i.e. a covalent bond, and this new bond is involved in a six-membered cyclic structure for which its associated ring critical point (rcp) is localized. After this point, ρ_b and *DI* increase progressively, $\nabla^2\rho_b$ becomes more negative and ε remains close to zero at the C_1-C_3 bcp, which indicates that this bond is being strengthened. C_1-B bond breaking occurs more delayed and progressively during the course of the reaction. In **Cm-p-3** structure, it can be clearly visualized that the charge concentration region around the C_1-B bcp is slimmer than that in **Cm-p-1** denoting the weakness of the C_1-B bond. Then, at the C_1-B bcp ρ_b and *DI* decrease up to values of 0.028 au. and 0.10, $\nabla^2\rho_b$ shows a small positive value (0.035 au.) and ε increases abruptly up to a value of 0.66 at **Cm-p-4** which indicates that the C_1-B covalent bond disappears at this stage.

Topological analysis of relevant points on the IRC of path D with *meta* orientation. In the pathway from enyne **5** to **TSD-m** the charge density is concentrated around the C_1-B bcp to form the covalent bond, in contrast to pathway C in which the C_1-B bond is breaking (See Fig. 5).[56] The C_1-B covalent bond is involved in the six-membered ring structure (**Dm-r-4**, see the ESI) like in **Cm-p-1**. Then, the C_1-C_3 interaction begins to weaken, as can be seen in **Dm-r-3**, in which the region of the charge concentration around the C_1-C_3 bcp is slimmer. In **Dm-r-2**, the C_1–C_3 interaction shows features of a closed shell interaction (ρ_b =0.087 au., $\nabla^2\rho_b$ = 0.056 au., and ε =1.2), in which the bond path that connects both atoms is bend around the C_1-C_2 bcp. In addition, in this structure *DI* C_1–C_3 (0.41) is similar to *DI* C_2–C_3 (0.40), reflecting that C_1 and C_2 are sharing the same amount of charge density with C_3. Then, in **Dm-r-1**, the C_1-C_3 bcp disappears and the C_1-C_2 bcp appears forming a cyclic seven-membered ring structure, in which *DI* C_1–C_3 (0.36) is now lower than DI C_2–C_3 (0.44). These results put forward that in the region among C_1, C_2 and C_3 a significant redistribution of the charge density occurs, and suggests that the system should pass by a conflict structure in which a bond path is linking C_3 and the C_1-C_2 bcp.[57] Therefore, these important finding reveals that the conflict state is the key point in the evolution of a six-member ring zwitterionic species towards a seven-member zwitterion structure.

RSC Advances Accepted Manuscript

Please do not adjust margins

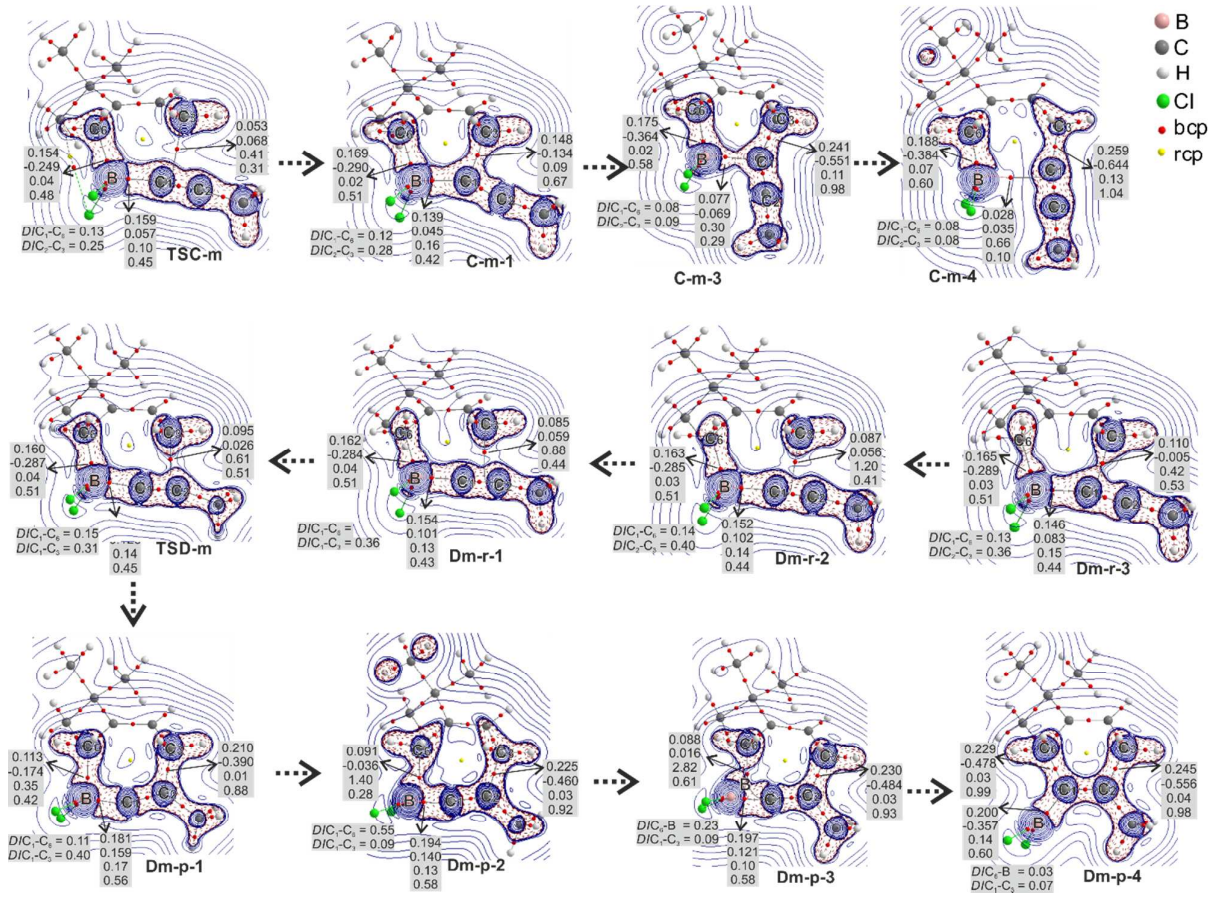

Fig. 5 Contour plots of - $\nabla^2\rho_b$ r superimposed on the molecular graphs of selected structures along the IRCs of **TSC-m** and **TSD-m**. Continuous blue lines and dashed red lines depict regions of local charge density depletion and concentration, respectively. The values given for selected bcps, from top to bottom, are ρ_b, $\nabla^2\rho_b$, ε and *DI*. DI of other interactions are also included. All symbols are explained in the text and the localization of structures on IRCs are shown in Figures 3 and 4.

In **TSD-m**, the C_6-B interaction is still a covalent interaction (ρ_b = 0.160 au., $\nabla^2\rho_b$ = -0.287 au., and *DI* = 0.51 at the C_6-B bcp) and the C_2-C_3 interaction is stronger than in the previous structure but still has features of an open shell interaction (ρ_b = 0.095 au., $\nabla^2\rho_b$ = 0.026 au., *DI* = 0.51). Also, DI C_1-C_6 and DI C_1-C_3 (0.15 and 0.31, respectively) indicate that these atoms are sharing their electrons too. This topology is in accordance with a [4 + 3] structure.[24] **TSD-m** and **TSB-m** have similar topological patterns but in the former, the electron density shared among the atoms of the diene and dienophile is greater than in the second (see the ESI). Therefore, we infer that the conflict state near the TS, in which the C_1 and C_2 atoms are closer to C_3, facilitates the sharing of electrons and as a consequence **TSD-m** structure is more stabilized.

After **TSD-m**, firstly the C_2-C_3 bond formation occurs being almost completely formed at **Dm-p-1** in which the C_2-C_3 bcp shows features of a covalent interaction (ρ_b = 0.210 au., $\nabla^2\rho_b$ = -0.390 au., ε= 0.01 and *DI* 0.88) and is involved in a seven-membered ring structure. At **Dm-p-2** the C_6-B bond begins to weaken (ρ_b = 0.019 au., $\nabla^2\rho_b$ = -0.036 au.,ε = 1.40 and *DI* 0.28) and the C_1-C_6 interaction starts to become stronger (*DI* C_1-C_6 = 0.55) although its corresponding bcp does not appear yet. In the following structure of the reaction path **Dm-p-3**, the C_6-B bcp disappears and the C_1-C_6 bcp is localized indicating the C_6-B bond breaking and the beginning of the C_1-C_6 bond formation in this stage of the reaction. A feature of the conflict stage is the larger value of the ε, such as in the C_1-C_6 bcp of **Dm-p-3** structure (ε = 2.82) denoting an asymmetrical distribution of the charge density around the bcp and the instability of the interaction. Therefore, these findings also indicate that the system undergoes a conflict mechanism, in which the B and C_1 atoms are competing to be bound to the C_6 atom and this is the basis for the evolution of the [4 + 3] structure toward the [4 + 2] structure.[24] At **Dm-p-4**, the C_1-C_6 interaction becomes stronger and has features of a covalent bond (ρ_b = 0.229 au., $\nabla^2\rho_b$ = -0.478 au., ε = 0.03 and *DI* 0.99) forming part of the six-membered ring structure as it is found in the final cycloadduct.

Conclusions

The reaction of dichloropropynylborane (**1**) with 2-*tert*-butylbutadiene (**2**) has been studied using density functional theory and the QTAIM approach in DCM in order to rationalize the mechanisms associated with the competing DA and AB reactions, and the origin of the experimental regioselectivity.

This journal is © The Royal Society of Chemistry 20xx

RSC Advances Accepted Manuscript

Please do not adjust margins

Three pathways (**A**, **B** and **C**) for each possible regioisomer, *meta* and *para*, were found. Pathways **A** and **B** correspond to the DA reaction and pathways **C** correspond to the AB process. For pathways A the mechanism are concerted and their **TSA**s associated have relatively high energy barriers and do not explain the experimental regioselectivity.

Pathways **B** and **C** correspond to stepwise mechanisms and share the first step of the reaction to the intermediate structures **IN-m** and **IN-p**. The second step is determinant for the reaction and involves [4 + 3] TSs, **TSB-m** and **TSB-p**, for pathways **B** and **TSC-m** and **TSC-p** for pathways **C**. The *meta* TS associated with the **C** pathway (**TSC-m**) is the most energetically favored structure among the TSs predicting the almost exclusive formation of the *meta* enyne under kinetic control, in agreement with the experimental results. The energy barriers of **TSB-m**, **TSB-p** and **TSC-p** were very similar, which demonstrates that the formation of the *meta* DA cycloadducts does not take place through **TSB-m**.

A TS which connects the enyne **5** with the DA cycloadduct **3** was found (**TSD-m**) and two plateau regions related with the six-membered and seven-membered ring structures were located in the associated reaction coordinate. **TSD-m** also has [4 + 3] character and a lower activation free energy than **TSC-m**. As cycloadducts were computed to be more stable than the corresponding enynes we propose that at longer reaction times the formation of the *meta* [4 + 2] cycloadduct might occur under thermodynamic control from enyne **5** *via* **TSD-m** passing by a six-membered ring structure and a seven-membered ring structure.

The topological analysis of the charge density distribution revealed that in the reaction pathway that connects enyne **5** with **TSD-m**, the system passes by a conflict structure in which a bond path is connecting C_3 with the C_1-C_2 bcp. This conflict mechanism is the key point in the evolution of a six-membered ring zwitterionic species towards a seven-membered zwitterion. Then, the [4 + 3] **TSD-m** progresses to the [4 + 2] cycloadduct by another conflict structure in which the B and C_1 atoms are competing to be bound to the C_6 atom.

Acknowledgements

We thank CONICET and ANPCyT. M. M. V. thanks UNNE, and SECYT-UNNE. S. C. P. thanks UNR.

Notes and references

1. G. Hilt and P. Bolze, *Synthesis*, 2005, 2091-2115.
2. G. Hilt, S. Lüers and K. I. Smolko, *Org. Lett.*, 2004, **7**, 251-253.
3. G. Hilt and K. I. Smolko, *Angew. Chem. Int. Ed.*, 2003, **42**, 2795-2797.
4. D. G. Hall, Boronic acids: preparation and applications in organic synthesis, medicine and materials, Wiley-VCH, Weinheim, 2nd completely rev. edn., 2011.
5. D. F. P. Crépin, J. P. A. Harrity, J. Jiang, A. J. H. M. Meijer, A.-C. M. A. Nassoy and P. Raubo, *J. Am. Chem. Soc.*, 2014, **136**, 8642-8653.
6. D. L. Browne, J. F. Vivat, A. Plant, E. Gomez-Bengoa and J. P. A. Harrity, *J. Am. Chem. Soc.*, 2009, **131**, 7762-7769.
7. P. M. Delaney, D. L. Browne, H. Adams, A. Plant and J. P. A. Harrity, *Tetrahedron*, 2008, **64**, 866-873.
8. E. Gomez-Bengoa, M. D. Helm, A. Plant and J. P. A. Harrity, *J. Am. Chem. Soc.*, 2007, **129**, 2691-2699.
9. P. M. Delaney, J. E. Moore and J. P. A. Harrity, *Chem. Commun.*, 2006, DOI: 10.1039/b607322k, 3323-3325.
10. M. D. Helm, J. E. Moore, A. Plant and J. P. A. Harrity, *Angew. Chem. Int. Ed.*, 2005, **44**, 3889-3892.
11. V. Gandon, C. Aubert and M. Malacria, *Curr. Org. Chem*, 2005, **9**, 1699-1712.
12. V. Gandon, C. Aubert and M. Malacria, *Chem. Commun.*, 2006, 2209-2217.
13. J. A. Sáez, M. Arnó and L. R. Domingo, *Tetrahedron*, 2003, **59**, 9167-9171.
14. N. Grimblat and S. C. Pellegrinet, *Org. Biomol. Chem.*, 2013, **11**, 3733-3741.
15. J. Jiao and Y. Nishihara, *J. Organomet. Chem.*, 2012, **721–722**, 3-16.
16. D. A. Singleton and S. W. Leung, *J. Org. Chem.*, 1992, **57**, 4796-4797.
17. S.-W. Leung and D. A. Singleton, *J. Org. Chem.*, 1997, **62**, 1955-1960.
18. Experimental data were reported for the reaction after the protodeboronation. Based on the Singleton`s work (ref 17) the same results for the borane products are considered.
19. M. A. Silva, S. C. Pellegrinet and J. M. Goodman, *J. Org. Chem.*, 2002, **67**, 8203-8209.
20. M. A. Silva, S. C. Pellegrinet and J. M. Goodman, *J. Org. Chem.*, 2003, **68**, 4059-4066.
21. F. Carreaux, F. Possémé, B. Carboni, A. Arrieta, B. Lecea and F. P. Cossío, *J. Org. Chem.*, 2002, **67**, 9153-9161.
22. R. F. W. Bader, *Atoms in Molecules. A Quantum Theory*, Oxford Science Publications, Clarendon Press, London 1990.
23. C. F. Matta and R. J. Boyd, The Quantum Theory of Atoms in Molecules: from solid state to DNA and drug design, Wiley-VCH, Weinheim, 2007.
24. M. M. Vallejos, N. M. Peruchena and S. C. Pellegrinet, *Org. Biomol. Chem.*, 2013, **11**, 7953-7965.
25. M. M. Vallejos, N. Grimblat and S. C. Pellegrinet, *J. Phys. Chem. A*, 2014, **118**, 5559-5570.
26. N. H. Werstiuk and W. Sokol, *Can. J. Chem.*, 2008, **86**, 737-744.
27. E. C. Brown, R. F. W. Bader and N. H. Werstiuk, *J. Phys. Chem. A*, 2009, **113**, 3254-3265.
28. J. E. Rode and J. C. Dobrowolski, *Chem. Phys.Lett.*, 2007, **449**, 240-245.
29. J. E. Rode and J. C. Dobrowolski, *J. Phys. Chem. A*, 2006, **110**, 207-218.
30. J. E. Rode and J. C. Dobrowolski, *J. Phys. Chem. A*, 2006, **110**, 3723-3737.
31. C. S. López and Á. R. d. Lera, *Curr. Org. Chem*, 2011, **15**, 3576-3593.
32. C. S. López, O. N. Faza, F. P. Cossío, D. M. York and A. R. de Lera, *Chem. Eur. J.*, 2005, **11**, 1734-1738.
33. G. Wagner, T. N. Danks and V. Vullo, *Tetrahedron*, 2007, **63**, 5251-5260.
34. S. Calvo-Losada and J. J. Quirante Sánchez, *J. Phys. Chem. A*, 2008, **112**, 8164-8178.
35. M. Zalazar and N. Peruchena, *J. Mol. Model.*, 2011, **17**, 2501-2511.
36. C. Lee, W. Yang and R. G. Parr, *Phys. Rev. B*, 1988, **37**, 785-789.
37. A. D. Becke, *J. Chem. Phys.*, 1993, **98**, 5648-5652.
38. E. Goldstein, B. Beno and K. N. Houk, *J. Am. Chem. Soc.*, 1996, **118**, 6036-6043.
39. K. N. Houk, J. Gonzalez and Y. Li, *Acc. Chem. Res.*, 1995, **28**, 81-90.

RSC Advances Accepted Manuscript

Please do not adjust margins

40. O. Wiest, D. C. Montiel and K. N. Houk, *J. Phys. Chem. A*, 1997, **101**, 8378-8388.
41. J. I. García, V. Martínez-Merino, J. A. Mayoral and L. Salvatella, *J. Am. Chem. Soc.*, 1998, **120**, 2415-2420.
42. D. M. Birney, *J. Am. Chem. Soc.*, 2000, **122**, 10917-10925.
43. J. Tomasi and M. Persico, *Chem. Rev.*, 1994, **94**, 2027–2094.
44. E. Cancès, B. Mennucci and J. Tomasi, *J. Chem. Phys.* , 1997, **107**, 3032-3041.
45. M. Cossi, V. Barone, R. Cammi and J. Tomasi, *Chem. Phys.Lett.*, 1996, **255**, 327-335.
46. V. Barone, M. Cossi and J. Tomasi, *J. Comput. Chem.* , 1998, **19**, 404-417.
47. M. J. T. Frisch, G. W.; Schlegel, H. B.; Scuseria, G. E.; Robb, M. A.; Cheeseman, J. R.; Scalmani, G.; Barone, V.; Mennucci, B.; Petersson, G. A.; Nakatsuji, H.; Caricato, M.; Li, X.; Hratchian, H. P.; Izmaylov, A. F.; Bloino, J.; Zheng, G.; Sonnenberg, J. L.; Hada, M.; Ehara, M.; Toyota, K.; Fukuda, R.; Hasegawa, J.; Ishida, M.; Nakajima, T.; Honda, Y.; Kitao, O.; Nakai, H.; Vreven, T.; Montgomery, J. A., Jr.; Peralta, J. E.; Ogliaro, F.; Bearpark, M.; Heyd, J. J.; Brothers, E.; Kudin, K. N.; Staroverov, V. N.; Kobayashi, R.; Normand, J.; Raghavachari, K.; Rendell, A.; Burant, J. C.; Iyengar, S. S.; Tomasi, J.; Cossi, M.; Rega, N.; Millam, N. J.; Klene, M.; Knox, J. E.; Cross, J. B.; Bakken, V.; Adamo, C.; Jaramillo, J.; Gomperts, R.; Stratmann, R. E.; Yazyev, O.; Austin, A. J.; Cammi, R.; Pomelli, C.; Ochterski, J. W.; Martin, R. L.; Morokuma, K.; Zakrzewski, V. G.; Voth, G. A.; Salvador, P.; Dannenberg, J. J.; Dapprich, S.; Daniels, A. D.; Farkas, Ö.; Foresman, J. B.; Ortiz, J. V.; Cioslowski, J.; Fox, D. J. , *Journal*, 2009.
48. T. A. Keith, *AIMAll, Version 11.12.19; TK Gristmill Software:Overland Park , USA, 2011*.
49. The TSs are named as follows: **TSA** and **TSB** for the TSs of the cycloaddition pathways; **TSC** for the TSs of the alkynylboration. With TS and IN indicate the TSs and intermediate structures corresponding to the first step of the reaction which are common to pathways **B** and **C**. Letters m or p indicate the *meta* or *para* regiochemistry.
50. Ratios were computed using Boltzmann factors based on $\Delta G^{\#}$
51. C. E. Check and T. M. Gilbert, *J. Org. Chem.*, 2005, **70**, 9828-9834.
52. G. O. Jones, V. A. Guner and K. N. Houk, *J. Phys. Chem. A*, 2006, **110**, 1216-1224.
53. G. A. Griffith, I. H. Hillier, A. C. Moralee, J. M. Percy, R. Roig and M. A. Vincent, *J. Am. Chem. Soc.*, 2006, **128**, 13130-13141.
54. Y. Zhao and D. G. Truhlar, *J. Phys. Chem. A*, 2004, **108**, 6908-6918.
55. In Figure 4, labels **r** and **p** indicate the point on the IRC corresponding to the path connecting the TS with the reactant or product, respectively.
56. Several structures corresponding to this part of the IRC are given in the ESI because of they are almost similar to those show in Fig. 5 associated with pathway **C**.
57. R. F. W. Bader, T. T. Nguyen-Dang and Y. Tal, *Rep. Prog. Phys.* , 1981, **44**, 893-948.

RSC Advances Accepted Manuscript

This journal is © The Royal Society of Chemistry 20xx